

VIBRATIONAL LIFETIME OF INTERSTITIAL OXYGEN IN CRYSTALLINE SILICON

Andrew Fraser

Department of Physics, The College of William and Mary

(April 24, 2002)

The lifetime of the antisymmetric stretch mode of interstitial oxygen in crystalline Si is measured directly by time-resolved, transient bleaching spectroscopy to be $T_l = 229 \pm 16$ ps at 10 K. The temperature dependence of the lifetime shows that the stretch mode decays into eight vibrational modes of 142 ± 20 cm⁻¹. The low-temperature width of the FTIR (IR) absorption line due to the stretch mode is 20 times broader than its natural width derived from the lifetime. This homogeneous broadening arises from phase relaxation induced by the coupling between the stretch mode and low-frequency bending modes.

PACS: 63.20.Pw, 78.47.+p

CONTENTS

- I. Introduction
- II. Theory
 - a. Harmonic Oscillator
 - b. Multi-Phonon Relaxation
- III. Experimental
 - a. Infrared Absorption Spectroscopy
 - b. Transient Bleaching Experiment
- IV. Results and Discussion
 - a. Lifetime Measurements
 - b. Decay Channel
 - c. Phase Relaxation
- V. Conclusion
- VI. Acknowledgement
- VII. References

I. INTRODUCTION

The study of relaxation dynamics of impurity vibrations down to the picosecond timescale resolution is an emerging field [1]. Such studies are only now becoming possible because of improvements in ultrafast infrared (IR) laser technology which allow lifetime measurements to be performed in the time domain. They will facilitate a better understanding of the vibrational dynamics and pathways of energy transfer at impurity sites. In particular, vibrational relaxation should affect the reactivity of impurities and their diffusion and desorption rates. This information is of interest to the semiconductor industry because it describes the durability of wafers made of silicon (Si), gallium arsenide (GaAs), and germanium (Ge) when carrying electric current. Defects in these crystals, such as lattice vacancies and interstitials, as well as impurities such as hydrogen (H), oxygen (O), carbon (C), and nitrogen (N), greatly alter their electrical properties. These impurities which are lighter than the host-lattice atoms give rise to local vibrational modes (LVMs) with frequencies above the phonon bands of the crystal. Depending on the details of the lattice location of the defect or impurity atom, particularly on symmetry and on how many bonds are formed with host lattice atoms, one observes a number of normal vibrational modes with well defined frequencies. Measuring the lifetime of the first excited states of the local vibrational modes elucidates these defect properties.

As with the earlier relaxation studies for condensed-matter phases, one can expect that the number of decay channels for a particular excitation increases strongly with the molecular complexity. Therefore, in order to make inroads into this previously unexplored field, one should look at the simplest and best characterized systems.

Oxygen in silicon was one of the first impurities in a solid studied by vibrational spectroscopy [3]. In an early work, Kaiser et al. [4] measured the temperature-dependent infrared absorption spectrum of oxygen in silicon. In their proposed model, the oxygen atom occupies an interstitial position, bonded to two Si neighbors. A schematic of the Si_2O defect is shown in Fig. 1.

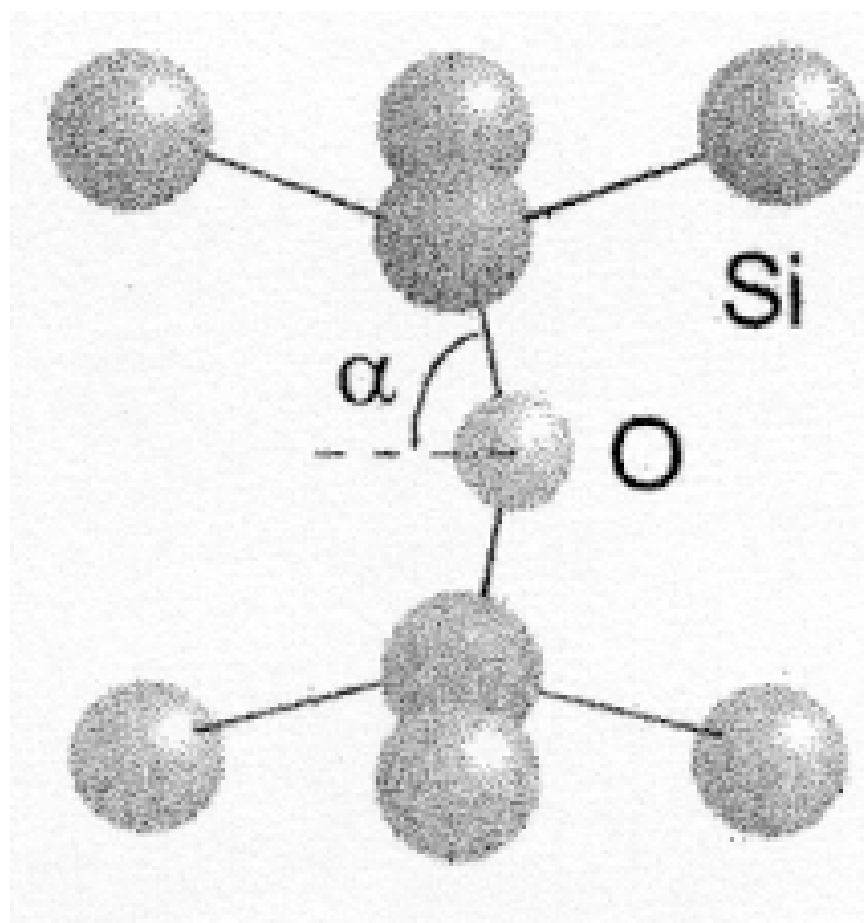


Figure 1: Structure of the Si_2O defect, including the 6 second-nearest neighboring Si atoms of the Si crystal. The oxygen impurity atom is shown in the center while all of the other atoms are silicon. Courtesy of McCluskey [5].

This structure gives rise to local vibrational modes (LVMs) that vibrate in excited energy states that are above the phonon bands of crystalline silicon. Figure 2 illustrates the possible LVMs of the oxygen defect in Si.

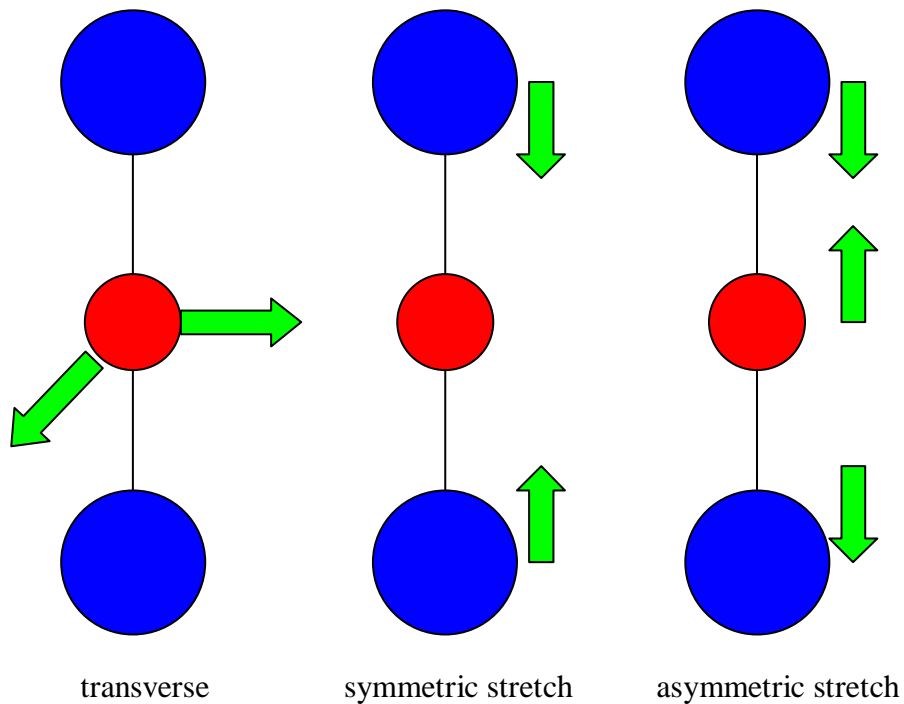


Figure 2: Local vibrational modes of the Si_2O and Ge_2O defects.

Hrostowski et al. [6] characterized one of the most prominent absorption bands (1136-cm^{-1} absorption band) as the antisymmetric stretch (alternatively called the asymmetric stretch) mode. It was also observed that there are a few side bands on the low-energy side of the 1136-cm^{-1} line when the temperature was raised above 20 K [7]. In subsequent models built by D. R. Bosomworth [7] and H. Yamada-Kaneta [8] explained that the stretch mode is coupled to a two-dimensional low energy anharmonic transverse (bending) mode of 29-cm^{-1} . Even though these models that were constructed from frequency-domain measurements have built a detailed understanding of the oxygen

absorption bands, the dynamics and relaxation channels of the oxygen LVM have remained previously unexplored.

Our research reports the first measurements of the vibrational lifetime of interstitial oxygen (denoted: 'O_i') in crystalline silicon. We report three significant results: I) The lifetime of the antisymmetric stretch mode is measured to be $T = 229 \pm 16$ ps at 10 K. The lifetime is more than one order of magnitude longer than for the stretch mode of interstitial-like hydrogen defects in silicon [9][10]. II) The temperature dependence of the lifetime shows that the stretch mode decays into eight vibrational modes of $142 \pm 20 \text{ cm}^{-1}$ corresponding to silicon TA phonons. The high order of the multi-phonon relaxation channel explains the long lifetime of the 1136-cm^{-1} mode. III) The homogeneous linewidth of the 1136-cm^{-1} line at 10 K is 20 times broader than its natural width derived from the vibrational lifetime. This broadening arises from pure dephasing due to the coupling between the stretch mode and low-frequency bending modes.

II. THEORY

This section describes a classical model of a local vibrational mode. A quantum mechanical model is used to determine the multi-phonon relaxation rate, *i.e.*, inverse lifetime, of the LVM. Derivations of these classical and quantum mechanical equations of motion are explained more comprehensively by McCluskey [5] and Nitzan *et al.*[11], respectively. The goal here is simply to explain how the lifetime of an LVM is calculated.

A) Harmonic Oscillator

Atoms in a crystalline solid collectively oscillate about their equilibrium positions, resulting in quantized vibrational modes, called phonons. The term *phonon* denotes excitations that are extended in real space and involve many atoms [12]. Phonons have a band of characteristic frequencies. Phonons in a perfect lattice have a well-defined frequency ω and normalized wave vector k . The relationship between ω and k , also called the dispersion of the phonons, can be measured by neutron scattering experiments. When an impurity is introduced in the lattice, the translational symmetry at the impurity site is broken and one or more vibrational modes may appear. If a defect of mass m replaces a heavier host atom of mass M , it will have vibrational modes with frequencies above the phonon bands. Unlike a phonon, the vibrational mode of the defect (impurity) is localized in real space. Therefore, it is called a *local vibrational mode* [5]. For example, interstitial Oxygen (O_i) typically has a stretching vibration (1136-cm^{-1} mode) that is ~ 2 times above the maximum phonon frequency of silicon (522-cm^{-1} transverse optical (TO) phonons) and has narrow infrared (IR) absorption peaks.

The classical model for a local vibrational mode of an impurity atom with relative charge q and mass m is an oscillating electric dipole [5]. Visually, it is analogous to a mass oscillating on a spring as shown in Fig. 3a. Its equation of motion is:

$$\frac{d^2x}{dt^2} + \gamma \frac{dx}{dt} + \omega_0^2 x = \frac{qE(t)}{\mu}, \quad (1)$$

where γ is the damping constant, $\omega_0 = \sqrt{K/\mu}$ is the natural angular frequency, $E(t)$ is the electric field as a function of time, $\mu = 1/[(1/m) + (1/M)]$ is the reduced mass, and M is the effective lattice mass.

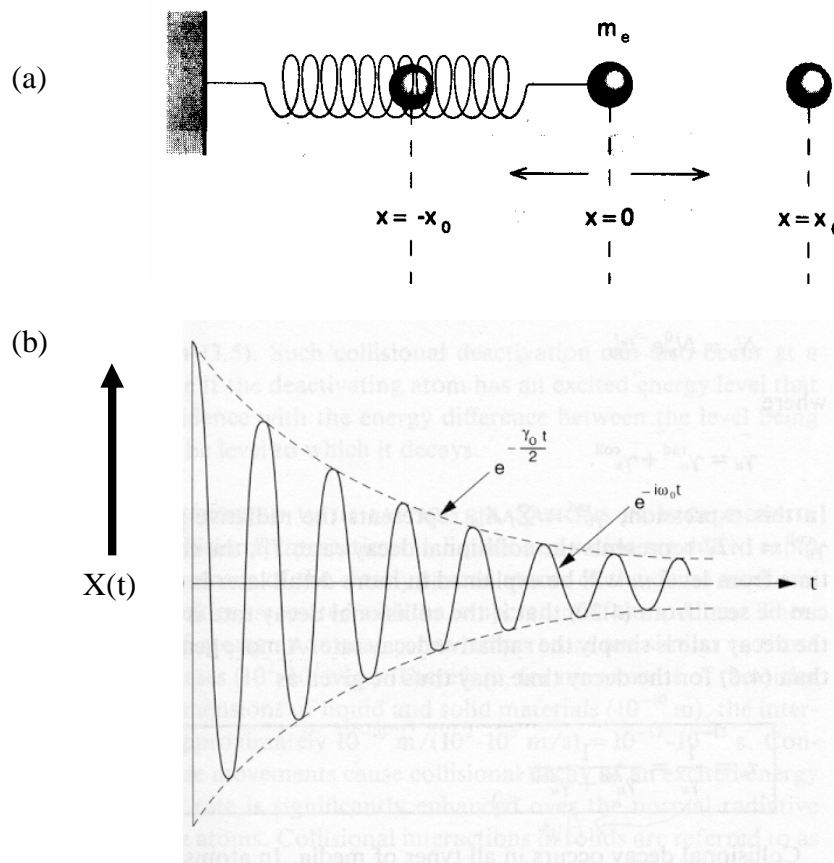


Figure 3: (a) Model of a mass oscillating on a spring; (b) decaying electric field of the damped harmonic oscillator. Courtesy of Silfvast [13].

The solution to Equation 1 is

$$x(t) = x_0 e^{i\omega_0 t - \gamma t/2}, \quad (2)$$

where the amplitude is given by

$$x_0 = \frac{qE_0/\mu}{\omega_0^2 - \omega^2 + i\gamma\omega}. \quad (3)$$

In Equation 3, E_0 is the electric field of the incident light. Figure 3b shows the decaying amplitude of the damped harmonic oscillator. The absorption cross section of radiation is given by the ratio of the power dissipation to the intensity of the electromagnetic wave [20][22]:

$$\sigma = \frac{\langle P \rangle}{ncE_0^2/8\pi} = \frac{4\pi q^2 \omega^2 \gamma}{n\mu c} \frac{1}{(\omega_0^2 - \omega^2)^2 + \gamma^2 \omega^2}. \quad (4)$$

The form of the absorption lineshape is known as a Lorentzian distribution (Fig. 4). The damping factor γ is approximately the full width at half maximum (FWHM) of the absorption peak. The shape of the absorption peak indicates whether the line is homogeneously or inhomogeneously broadened. A homogeneous line is distributed by the Lorentzian function according to Equation 4 [16]. An inhomogeneous line is

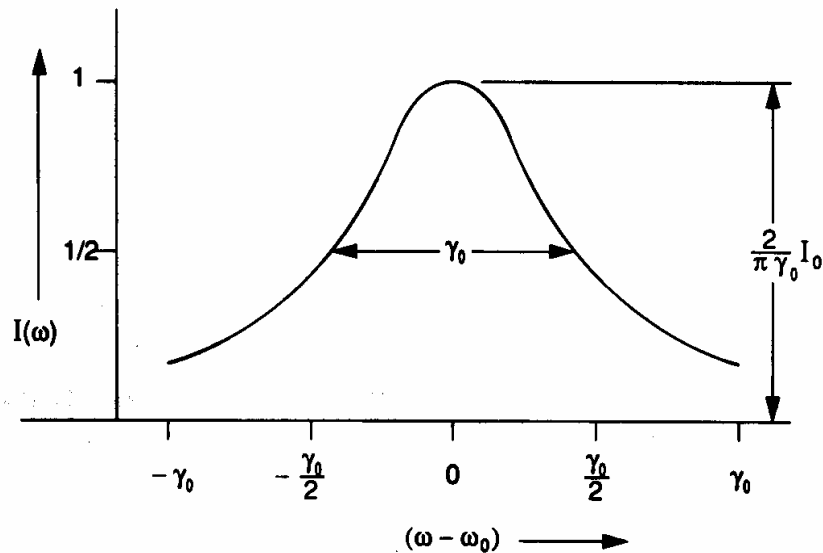


Figure 4: Lorentzian distribution of absorption intensity as a function of absorption frequency. Courtesy of Silfvast [13].

distributed by a Gaussian function (also called a Normal distribution) [16]. Often, an absorption line is broadened by both homogeneous and inhomogeneous factors; therefore the shape of an absorption line is generally refined by the convolution of its homogeneous line shape with a function describing the inhomogeneous broadening [13]. Inhomogeneous broadening results from strain fields induced by lattice defects present in the sample. If not all of the oxygen defect sites have the same structure (amorphous), then the absorption line of oxygen in silicon will be inhomogeneously broadened because the difference in defect structure causes slight variation in absorption frequencies. In this experiment, inhomogeneous broadening was minimized by using a low concentration of oxygen; therefore, the defects were spread out and were unlikely to deform each other. The good fit of a Lorentzian function to the oxygen absorption peak confirms that homogeneous broadening dominated. Generally, the homogeneous line width is given by

$$\gamma = \frac{1}{2\pi cT_1} + \frac{1}{\pi cT_2^*}, \quad (5)$$

where T_1 is the lifetime of the energy relaxation and T_2^* is the time of phase relaxation. The vibrational lifetime is usually a good estimate of the natural line width. The second term generally dominates the line width at elevated temperatures, due to elastic scattering

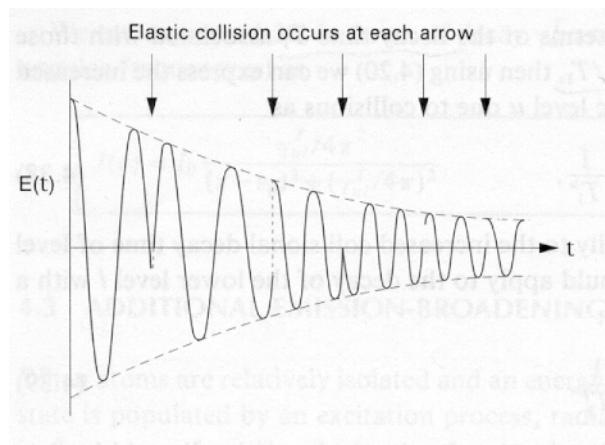


Figure 5: Phase interruptions (relaxation) of a decaying oscillation due to dephasing (inelastic) collisions. Courtesy of Silfvast [13] 10

of the local mode with the phonon bath. Figure 5 illustrates broadening due to collisional dephasing in the time domain [13].

B) Multiphonon Relaxation

The simplest quantum mechanical model for a local vibrational mode is the harmonic oscillator. It is a robust approximation for the first few excited vibrational levels of an impurity atom bonded to host atoms. However, there are anharmonic corrections due to the coupling between the LVM and the phonon bath, which can lead to a non-radiative decay mechanism of the LVM. If the energy of the LVM exceeds the maximum energy of a single phonon, then many phonons can be created simultaneously in the decay process. This process is known as multi-phonon relaxation. The Hamiltonian of this system [11] can be written as

$$H = H_{\text{LVM}} + H_{\text{BATH}} + H_{\text{INT}}. \quad (6)$$

In this Hamiltonian, H_{LVM} describes the two relevant quantum levels (initial and final) of the LVM, H_{BATH} is the Hamiltonian of the phonon bath (crystal lattice vibration), and H_{INT} describes the interaction between the LVM and the phonon bath. The more specific form of equation H_{LVM} [10] is

$$H_{\text{LVM}} = \hbar\omega a^\dagger a, \quad (7)$$

where the annihilation operator a is [14]

$$a = \frac{1}{\sqrt{2m}} \left(\frac{\hbar}{i} \frac{d}{dQ} + im\omega \right) \quad (8)$$

and the creation operator a^\dagger is

$$a^\dagger = \frac{1}{\sqrt{2m}} \left(\frac{\hbar}{i} \frac{d}{dQ} - im\omega \right). \quad (9)$$

Notice that Equations 7,8,9 are the equations of motion for the quantized (simple) harmonic oscillator. The variable Q represents the normal coordinate of the local mode of the defect atom of mass m . The symmetry of this normalized vibration is shown in Fig. 2. The Hamiltonian for the phonon bath is

$$H_{\text{BATH}} = \sum_{\{v\}} \sum_{i=1}^{N_v} \hbar\omega_i^{\{v\}} b_{i,\{v\}}^\dagger b_{i,\{v\}}, \quad (10)$$

with the annihilation operator

$$b_{i,\{v\}} = \frac{1}{\sqrt{2m}} \left(\frac{\hbar}{i} \frac{d}{dQ_{i,\{v\}}} + im\omega_i^{\{v\}} \right) \quad (11)$$

and the creation operator

$$b_{i,\{v\}}^\dagger = \frac{1}{\sqrt{2m}} \left(\frac{\hbar}{i} \frac{d}{dQ_{i,\{v\}}} - im\omega_i^{\{v\}} \right). \quad (12)$$

Each channel $\{v\}$ is characterized by the set $\{\omega_1^{\{v\}}, \omega_2^{\{v\}}, \dots, \omega_{N_v}^{\{v\}}\}$ of accepting mode frequencies. Energy is conserved in the decay process, *i.e.*: $\hbar\omega = \sum_{i=1}^{N_v} \hbar\omega_i^{\{v\}}$, where ω is the frequency of the LVM.

The Hamiltonian H_{INT} describes the coupling between the LVM and the phonon bath, which gives rise to an anharmonic perturbation to the harmonic H_{LVM} . The Hamiltonian describing the coupling between the LVM and the phonon bath is given by

$$H_{\text{INT}} = \sum_{\{v\}} \hbar(G_{\{v\}} B_{\{v\}} a^\dagger + G_{\{v\}}^* B_{\{v\}}^\dagger a), \quad (13)$$

where $G_{\{v\}}$ is the temperature-independent coupling strength and $B_{\{v\}}$ and $B_{\{v\}}^\dagger$ represent the product of the creation and annihilation operators for all of the decay channels, given by $B_{\{v\}}^\dagger = \prod_{i=1}^{N_{\{v\}}} b_{i,\{v\}}^\dagger$ and $B_{\{v\}} = \prod_{i=1}^{N_{\{v\}}} b_{i,\{v\}}$, respectively.

The coupling term H_{INT} gives rise to matrix elements which lead to only a small perturbation of the eigenvalues and eigenfunctions of H_{LVM} . Therefore, the complete Hamiltonian of the system, H , can be solved using first-order time-dependent perturbation theory [14]. The first-order correction terms lead to an anharmonicity of the vibrational levels which has two effects on the LVM: i) The spacing between energy levels decrease with increasing excited state, and ii) the energy width ΔE of the vibrational level is broadened due to the increase in the decay rate caused by the coupling to the phonon bath. The latter effect is a direct consequence of the Heisenberg Uncertainty Principle [13]:

$$\Delta E \Delta t \approx \hbar, \quad (14)$$

where $\Delta t \cong T_1$, i.e. the inverse of the decay rate γ . Figure 6 shows the relationship between the natural linewidth and the width of the energy levels.

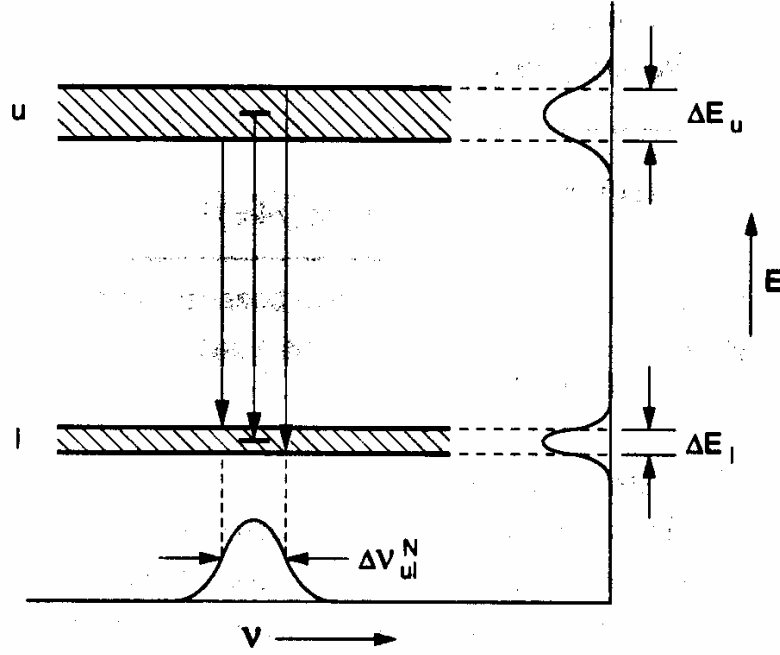


Figure 6: Quantum mechanical description of the natural linewidth resulting from the transition between the two levels. Courtesy of Silfvast [13].

The solution of Equation 6 obtained from time-dependent theory yields the decay rate

$$\gamma = \frac{1}{T_1} = \pi \sum_{\{v\}} |G_{\{v\}}|^2 n_{\{v\}} \rho_{\{v\}}. \quad (15)$$

In Equation 15, $n_{\{v\}}$ describes the thermal population (Bose-Einstein distribution) of accepting modes

$$n_{\{v\}} = \frac{e^{\hbar\omega/k_B T} - 1}{\prod_{\{v\}} e^{\hbar\omega_{\{v\}}/k_B T} - 1}, \quad (16)$$

and $\rho_{\{v\}}$ is the compound spectral density of accepting states. The function $n_{\{v\}}$ describes the temperature dependence of the decay rate. At low temperature, $n_{\{v\}} = 1$ and the LVM decays by spontaneous relaxation into N_v accepting modes. At elevated temperature, the relaxation rate increases due to stimulated emission by thermal population of the

accepting modes [11][16]. Experimentally, the accepting mode frequencies can be obtained from the temperature dependence of the lifetime of the LVM.

III. EXPERIMENTAL

A) Infrared Absorption Spectroscopy

Absorption measurements of the asymmetric stretch mode were taken using a Fourier-Transformed Infra-Red (FTIR) spectrometer. We used a Nicolet FTIR spectrometer with a maximum resolution of 0.125 cm^{-1} . Since its development in the 1970's, the FTIR-spectrometer has become a valuable tool for taking frequency domain vibrational spectra

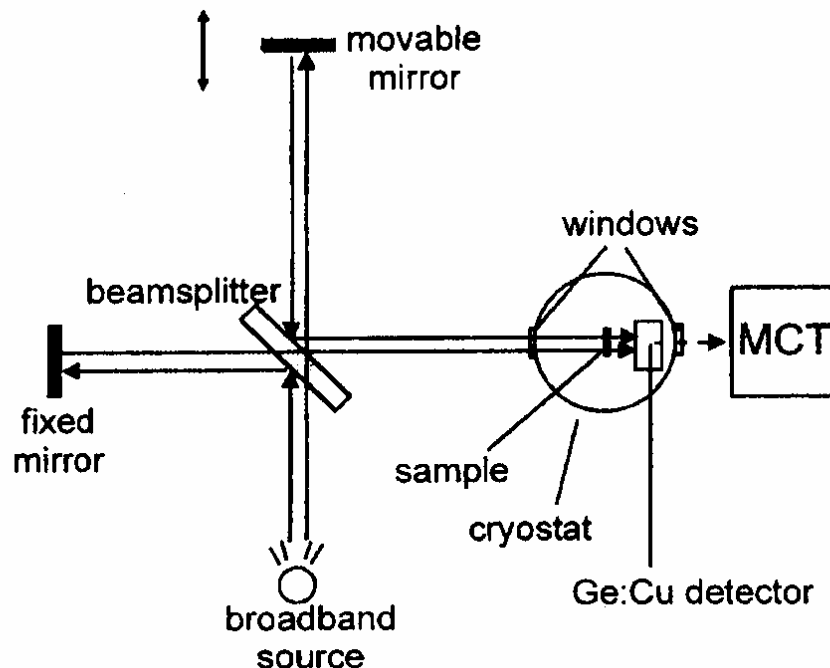


Figure 7: Schematic of an FTIR spectrometer. Courtesy of McCluskey [5]

because of its ability to scan over a broad range of IR wavenumbers (400-cm^{-1} - $\sim 10,000\text{-cm}^{-1}$) and produce low-noise spectra. The fundamental component of an FTIR

spectrometer is a Michelson Interferometer, which is shown in Fig. 7. The beamsplitter and the two mirrors comprise the interferometer. It splits a beam in two, varies the pathlength of the two beams, and then recombines them. This produces an interference pattern of maximum and minimum coherence which varies as the pathlength difference is changed. The broadband source is a globar IR source which emits uniform intensity blackbody radiation over all IR wavelengths. As a detector one can either use a Ge:Cu plate or a Mercury-Cadmium-Telluride (MCT) photodiode. The sample is placed into a cryostat, allowing its temperature to be varied by a cooling device (usually liquid He)

The initial spectrum taken by an FTIR, called an interferogram, gives the beam intensity as a function of the movable mirror position, $I(\delta/2)$. The interferogram is then apodized, using the Happ-Genzel function [15]. Apodization serves to smooth out any outlying peaks that are not part of the central interference peak. This apodized-interferogram is then Fourier-transformed such that the intensity as a function of distance (of the moveable mirror) function is transformed into intensity as a function of wavenumber $I(\sigma)$. Wavenumber, σ , is the preferred method of characterizing a wave on an FTIR spectrum, and is related to both wavelength, λ , and frequency, ν , by the equation: $\sigma = (1/\lambda) = (\nu/c)$. The mathematical expression for the Fourier transform of the interferogram, $I(\delta/2)$ is

$$I(\sigma) = \frac{2}{C_0} \int_0^{\infty} I(\delta/2) \cos[2\pi\bar{Z}\sigma] dz, \quad (17)$$

where $\delta/2$ is the position of the moveable mirror, $\bar{Z} = Z_2 - Z_1$ is the difference in optical pathlength of the two waves, and C is an instrumental constant. Since the Intensity versus mirror position is scanned into a computer as a matrix rather than as a continuous function, matrix manipulations must be used in lieu of equation (15); an FTIR

spectrometer uses a matrix operation algorithm called a Fast-Fourier-Transform for this operation. These steps yield a spectrum of intensity as a function of wavenumber. However, the spectrum is inherently corrupted by the conditions of the spectrometer, which yields instrumental absorbance peaks (caused by H₂O, CO₂, etc). Therefore, another scan is taken without the sample in order to reveal these instrumental absorption peaks. This interferogram is also apodized and Fourier-transformed, yielding a background spectrum I_B(σ). Lastly, the absorbance spectrum, Abs(σ), is calculated by

$$\text{Abs}(\sigma) = -\log_{10} \frac{I_B(\sigma)}{I(\sigma)}, \quad (18)$$

giving the spectrum in its uncorrupted form [15].

The FTIR absorbance peak of a defect contains much valuable information about its nature. The position of the peak (measured in wave-numbers: 1/λ) characterizes the defect (*e.g.*- asymmetric stretch). The LVM frequency is $\omega_0 = \sqrt{K/\mu}$. Impurities, such as H,C, O and N, which are lighter than the host atoms, for example Si or Ge, have LVMs with frequencies above the phonon bands of the crystal. Most defects in solids have already been characterized by FTIR spectroscopy (or more primitive Infra-Red spectroscopy methods) and vast libraries of this data are available [4][6][7].

B) Transient Bleaching Experiment

In the time domain, the lifetime of the asymmetric stretch mode is measured directly by transient-bleaching spectroscopy. In order to perform transient-bleaching spectroscopy, an infrared (IR) pump-probe apparatus was used. A schematic of the setup is shown in Fig. 8. The laser shown at right is a Spectra Physics Optical Parametric Amplifier (OPA Laser). It delivers pulses at a 1 kHz repetition rate with a pulse time duration of 130 fs,

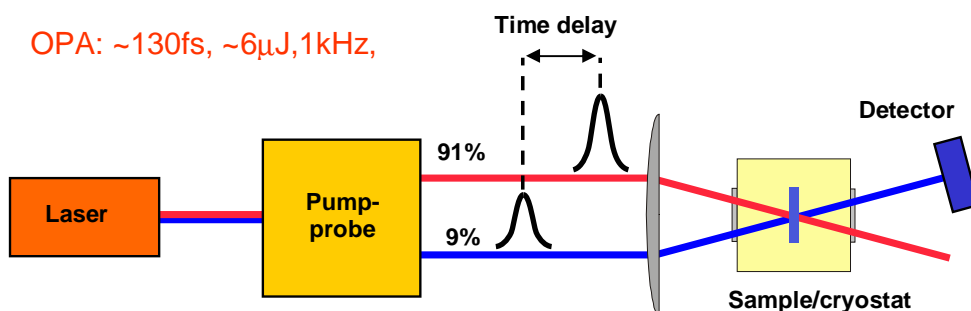


Figure 8: Schematic of the transient bleaching experiment.

spectral width of 177 cm^{-1} , pulse energy of $6\text{ }\mu\text{J}$, and center wavelength of $\lambda = 8.8\text{ }\mu\text{m}$ (1136 cm^{-1} in wavenumbers). The pump probe box in this diagram represents a beamsplitter that splits the laser pulse into two pulses and a series of mirrors attached to a moveable stage that varies the length over which one of the pulses travels. The first split pulse which contains $\sim 91\%$ of the original laser's intensity is the pump pulse. The second pulse which contains 9% of the intensity is the probe pulse. The probe's path length is varied by the stage. A measured change in pathlength can be expressed as a delay in arrival of the two beams by the relation: $\Delta t = \Delta L/c$, where Δt is the change in pulse arrival time, ΔL is the change in path length, and $c = 299792458.8 \pm .2\text{ m/s}$. The pump excites a fraction of the interstitial oxygen to the first excited state of the stretch mode, which causes the transmission coefficient of the sample to temporarily increase. This process, called transient bleaching, results in the temporary transparency of a defect to light at its LVM frequency. The transient bleaching signal S_b is monitored with the probe beam as the beam path difference between the pump and probe is varied. If a probe beam follows immediately after the pump, almost all of its intensity will be retained as it passes through the material and appears as a signal spike on a photo-

detector. As the excited mode decays back to the ground state the transmission coefficient returns to its original value and the probe signal returns to its original value.

The signal S_b is detected using an amplified liquid nitrogen-cooled HgCdTe detector. To allow for temperature-dependent measurements, all experiments are performed with the sample mounted in an optical vacuum cryostat. The sample is a 3-mm thick, disk-shaped, Si single crystal, grown by the Czochralski (CZ) method, which yields a high uniform O_i concentration of $\sim 8 \times 10^{17} \text{ cm}^{-3}$. The sample used for IRAS measurements is 5-mm thick and cut from a primary ingot grown by the Float Zone (FZ) method. The FZ sample contains a low O_i concentration of $\sim 6 \times 10^{16} \text{ cm}^{-3}$ as determined by IR absorption measurement.

IV. RESULTS & DISCUSSION

A) Lifetime Measurements

Figure 9 shows the transient bleaching signal S_b from the antisymmetric stretch mode as a function of time delay between the pump and probe pulses measured at 10 K. In Fig. 5, the data points are fitted to an exponential decay by the method of least squares. The signal decreases exponentially with a time constant of $T_l = 229 \pm 16$ ps. Since the laser spectrum has a FWHM of 177-cm^{-1} and the laser frequency is centered on the 1136-cm^{-1} absorption peak, the stretch modes at 1128 and 1122-cm^{-1} , and the combination mode at 1205 cm^{-1} also contribute to S_b . The lines at 1128 and 1122-cm^{-1} arise via nonlinear coupling between the stretch mode and the low-frequency bending modes which become thermally populated above liquid helium temperature [7]. The 1205 cm^{-1} mode is ascribed to a multi-quantum transition due to the coupling between the

asymmetric-stretch and bending modes [7]. The intensity of these absorption lines is at least one order of magnitude smaller than the 1136-cm^{-1} line at 10 K, and therefore they contribute very little to S_b . Similarly, the absorption lines at 1107 and 1084-cm^{-1} due to the O isotope effect are more than two orders of magnitude smaller. Additional lines from the ^{29}Si and ^{30}Si isotopes are also negligible. Moreover, S_b shows a single-exponential decay indicating that either the lifetime of all these modes must be very similar or their contribution to S_b is negligible compared to the stretch mode (1136-cm^{-1}).

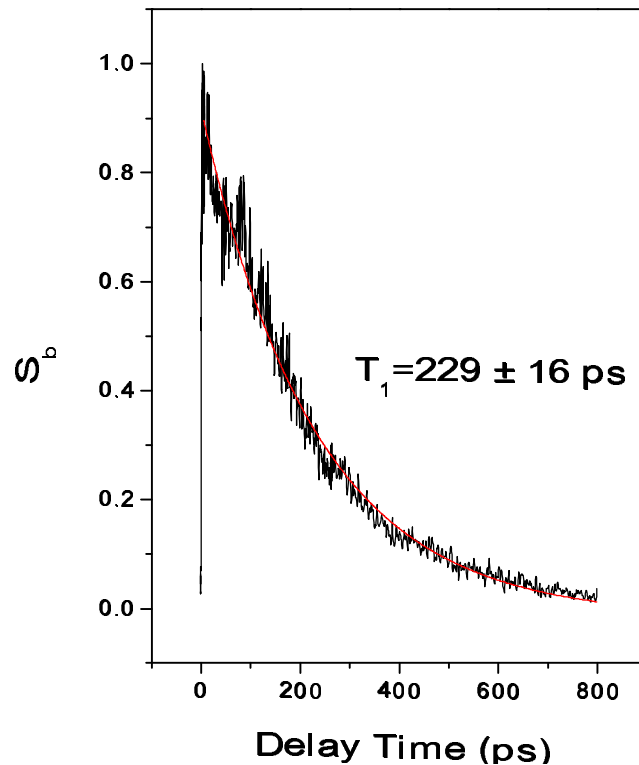


Figure 9: Transient bleaching signal from the 1136-cm^{-1} mode at 10 K.

B) Decay Channel

In order to understand the origin of the long lifetime of the stretch mode, knowledge of the LVM's decay channels is necessary. Because the vibrational quantum is smaller than the bandgap (*ie.* the decay of the LVM cannot excite an electrical current because it does not have enough energy to kick its valence electrons from the valence band into the conduction band) and the sample is cut from intrinsic Si (O_i is electrically inactive), electronic mechanisms are not possible. Therefore, the decay must occur via multi-phonon emission.

Experimentally, the accepting mode frequencies can be obtained from the temperature dependence of the lifetime of the LVM. At low-temperature, the vibrational lifetime is almost purely determined by spontaneous decay. The LVM breaks down into N_v accepting modes (lower energy LVMs at different center frequencies). At elevated temperature, the relaxation rate increases due to stimulated emission by thermal population of the accepting modes [11][16]. The selection rule of vibrational decay favors the process with the least amount of phonons. Figure 10 shows two different plots of lifetime as a function of temperature. All of the data points in Fig. 10 are plotted on a natural-logarithmic scale; therefore, exponential decay appears as a straight line (This method facilitates a linear least-squares fit). Figure 10a shows four superimposed plots of the transient bleaching lifetime signals at 50 K, 70 K, 90 K, and 110 K. Fig. 6b shows the fit of Equation 16 to the measured lifetimes at temperatures ranging from 10 K up to 120 K. Several lifetime measurements were performed at each temperature.

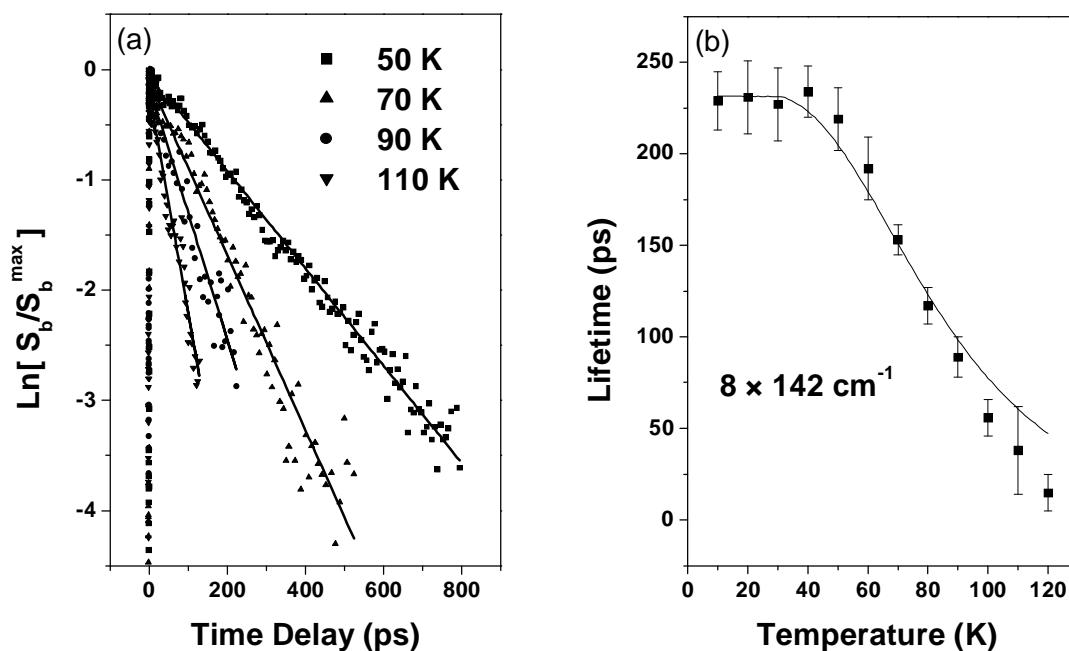


Figure 10: Temperature dependence of the lifetime. Fig. 10a shows $\log_e(S_b)$ for four different temperatures. Fig. 10b shows the fit of Equation 16 to all lifetimes.

The mean of each temperature measurement is shown by the squares and their standard deviations are shown by the error bars. In Fig. 10b, T_1 is nearly constant at ~ 229 ps up to 50 K, where it starts to decrease rapidly, approaching half of its low-temperature value at 70 K and reaching 20 ps at 120 K. As the temperature is raised above 20 K, the low-frequency bending modes become thermally populated, resulting in new modes (1128 and 1122-cm^{-1}) on the low-frequency side of the 1136-cm^{-1} mode. Figure 6a reveals that the transient bleaching signal has a uniform pattern of exponential decay at all temperatures indicating that the lifetime of these additional stretch modes must be very similar. This is also consistent with T_1 being nearly constant up to ~ 50 K, which puts a

lower boundary on the frequency of the accepting modes. The fact that the lifetime of the stretch mode decreases by more than one order of magnitude within a temperature range of 70 K shows that a high number of low-frequency accepting modes are involved in the decay channel. The solid line in Fig. 10b is a fit using Equations 15 and 16 with the vibrational relaxation channel of the 1136-cm^{-1} mode represented by a set of eight accepting modes of $142 \pm 20 \text{ cm}^{-1}$. Figure 10b shows that the fit of a single decay channel deviates from the measured T_l 's at elevated temperatures, indicating that additional relaxation channels may increase the decay rate at higher temperatures.

The decay channel provides an important clue in explaining the long lifetime of Si:O. The T_l is more than one order of magnitude larger than the lifetime of the stretch modes of interstitial-like hydrogen defects in silicon, for example the 1998-cm^{-1} mode of bond-center hydrogen has a lifetime of $T_l = 7.8 \pm 0.2 \text{ ps}$ [10]. This result is surprising, considering that the 1136-cm^{-1} mode has nearly half the vibrational energy of the 1998-cm^{-1} mode of bond-centered hydrogen. Consequently, the order of the decay process, *ie.*, the number of phonon modes into which the LVM decays, can be smaller for O_i than bond-centered hydrogen. The critical difference between these defects is their local structure gives rise to both a very different local vibrational mode structure, referred to as pseudolocalized modes (PLMs), and very different anharmonic coupling strengths, G_v . The fact that T_l is nearly constant up to 50 K shows that the bending modes at $\sim 29\text{-cm}^{-1}$ contribute little to the decay rate. Furthermore, a decay channel involving transverse pseudolocalized modes at $\sim 518\text{-cm}^{-1}$ is also not compatible with the strong temperature dependence of the lifetime [6][7]. Since the O_i atom can move relatively unhindered in

the plane perpendicular to the bond axis [22], it seems plausible that a transverse motion of O_i or of the neighboring Si atoms has little effect on the lifetime of the stretch mode. The nature of the low-frequency accepting modes of $142 \pm 20 \text{ cm}^{-1}$ is not known. However, likely candidates are transverse acoustic (phonon bath) phonons and/or pseudolocalized resonant modes of O_i . We note that the accepting modes nearly coincide with the peak in the density of TA phonons of the undistorted Si crystal [23]. The peak at 150-cm^{-1} arises from TA phonon bands with a flat dispersion in the [100] or [110] directions. Evidently it is the phonon modes or PLMs with a longitudinal displacement of the Si atoms along the bond axis that govern the lifetime of the 1136-cm^{-1} mode. To explain the long lifetime, it is necessary to consider also the anharmonic coupling strength. The $G_{\nu s}$ are proportional to the derivative of the potential energy surface with respect to the normal coordinates of the LVM and the N_{ν} accepting modes, corresponding to anharmonic terms of order $N_{\nu} + 1$ [11][16]. Since the magnitude of the anharmonic terms is believed to fall off rapidly with increasing order, channels with a high number of accepting modes, such as the 1136-cm^{-1} mode, will have a small decay rate.

C) Phase Relaxation

Further information on the dynamics of the stretch mode can be obtained from FTIR spectroscopy (IRAS). From Equation 5 we estimate the natural linewidth of the stretch mode to be 0.023-cm^{-1} . Fig. 11 shows the absorption line from the antisymmetric stretch mode measured at 10 K. In order to avoid inhomogeneous broadening, a 5-mm thick FZ sample is used with an O_i concentration of less than 2 ppm. The absorption line is almost perfectly represented by a Lorentzian distribution (dotted line). The FWHM of the 1136-

cm^{-1} line is 0.55-cm^{-1} , which is 20 times broader than the natural linewidth derived from the lifetime! This is in strong contrast to hydrogen-related LVMs in silicon which approach the natural linewidth at low temperature (10 K) and low hydrogen concentration (1 ppm) [8]. To understand this surprising result we investigated the homogeneous linewidth of the antisymmetric stretch mode (855-cm^{-1} of O_i in Ge. A. J. Mayur et al. measured a FWHM of $0.02 \sim 0.04\text{-cm}^{-1}$ for Ge:O at 2 K [20]. A linewidth of 0.02-cm^{-1} yields a minimal lifetime of 265 ps which is very close to $T_l = 229 \pm 16$ ps measured for the 1136-cm^{-1} mode of Si:O. We expect the vibrational lifetime of the antisymmetric stretch mode of O_i to be very similar in Si and Ge, i.e. within a factor of two, since the lifetimes of LVMs are found to be comparable in these materials [21].

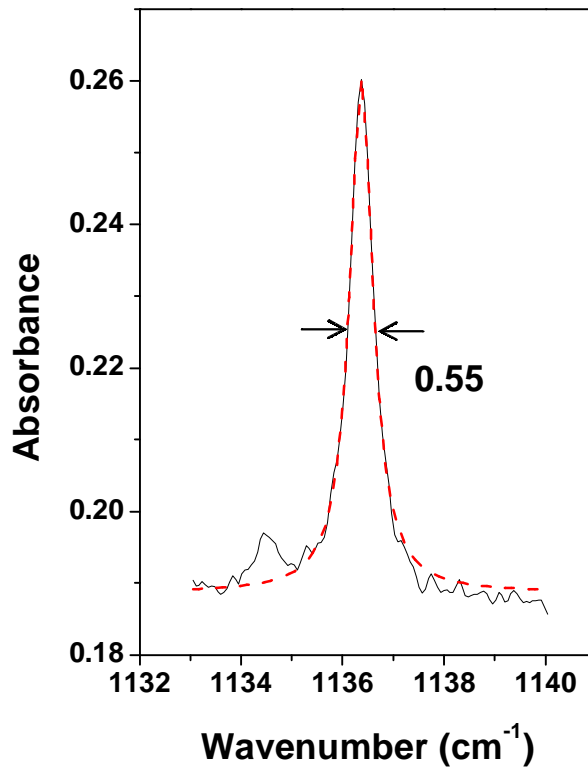


Figure 11: FTIR absorption peak of the asymmetric stretch mode of Si_2O at 10 K.

The structure of the interstitial oxygen defect, shown in Fig. 12, provides the key to explain the large low-temperature homogeneous broadening of the 1136-cm^{-1} line. Initial calculations estimated the Si-O-Si bond angle to be approximately $2\alpha = 170^\circ$ [22], while the Ge-O-Ge bond angle is $\sim 140^\circ$ [23]. The distance of the oxygen atom from [111] axis is 0.22 \AA for Si, while it is 0.58 \AA for Ge [23]. Both bond sites, Si_2O and Ge_2O , have an antisymmetric stretch mode and their coupling interactions lead to the unusual temperature-dependent fine structure of the stretch mode. The 855 cm^{-1} mode of Ge:O exhibits a very complex spectrum at low temperature with as many as 44 sharp lines within a 5-cm^{-1} range [24]. The fine structure can be explained as a consequence of a smaller binding angle of the Ge_2O quasi-molecule. The large distance of O_i from the

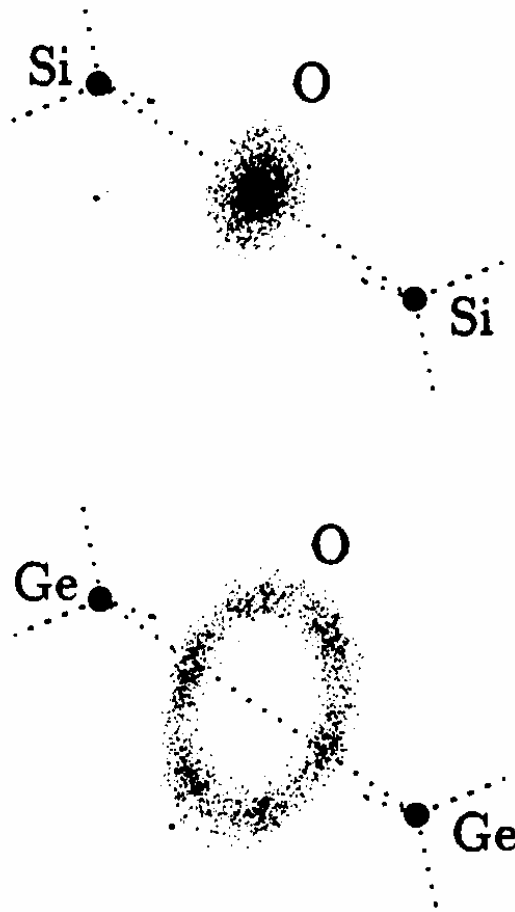


Figure 12: Structures of Si₂O and Ge₂O defects. Courtesy of Artacho [18].

[111] axis results from a strong central potential barrier (Fig. 13). The coupling between the 855-cm⁻¹ mode and a rigid rotator explains the complex fine structure spectrum of Ge:O at very low temperature. The Si₂O quasi-molecule, O_i shows a low-energy two-dimensional motion. From calculations of the energy barriers, M. A. Roberson *et al.* proposed that O_i in Si can in principle move through the bond center rather than around it [22].

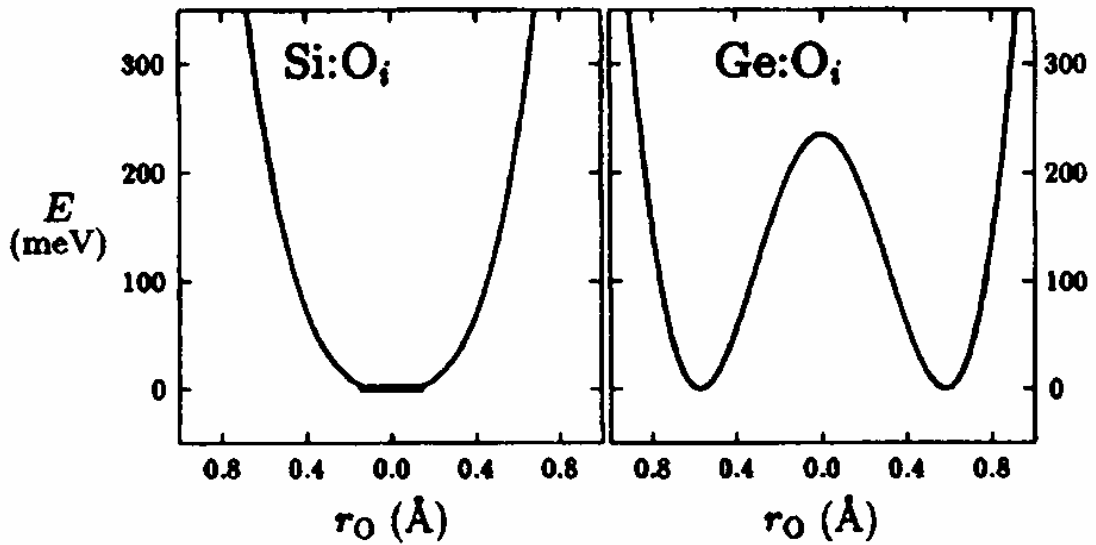


Figure 13: Hamiltonian potential wells of Si_2O and Ge_2O . Courtesy of E. Artacho [18]

The different motions of the interstitial oxygen leads not only to the different fine structures, but also to the large difference in the homogeneous linewidths. The potential of the stretch mode changes slightly with increasing distance of the O_i atom from the bond axis. This effect is observed theoretically [8] and experimentally [24]. Yamada-Kaneta, *et.al.* calculated the coupling constant G_v between the antisymmetric stretch and the low-frequency bending modes [8]. The negative value of G_v implies that the stretch mode frequency decreases as the oxygen atom moves off the bond axis. This effect was observed in silicon under hydrostatic pressure [24]. When pressure is applied, the silicon atoms exert a force on the O_i atom, causing it to move off center and the frequency of the stretch mode decreases. Thus the two-dimensional motion of the O_i atom in Si leads to a homogeneous broadening of the 1136-cm^{-1} line at low temperature. This motion does not increase the vibrational population relaxation rate, but causes homogeneous dephasing of the asymmetric stretch mode.

V. CONCLUSION

In summary, we have measured the vibrational lifetime of the asymmetric stretch mode of interstitial oxygen in Si to be $T_l = 229 \pm 16$ ps at low temperature, and have shown that the dominating decay channel involves eight low-frequency modes of 142 ± 20 cm^{-1} . The homogenous linewidth of the 1136-cm^{-1} mode at 10 K is 20 times broader than the natural width derived from the lifetime. The coupling between the stretch and the bending modes leads to the large homogeneous broadening of the 1136-cm^{-1} mode. These results indicate that the vibrational dephasing and lifetime are strongly dependent on the local defect configuration. Thus quantitative models of these processes require detailed knowledge of the local structure and the associated local phonons. The results presented here have great significance in excitation processes which involve the dynamics of energy dissipation in solids and will motivate further research regarding stability and diffusivity of impurities in semiconductors as well as complex formation.

VI. ACKNOWLEDGEMENT

The author acknowledges Baozhou Sun and Gunter Luepke as co-authors. Their input was invaluable to writing this undergraduate-level paper. We gratefully acknowledge S. A. Abrash for providing the FTIR equipment. This work was supported in part by NSF through grant DMR-00-76027, ONR through grant N00014-01-1-0770, and the Thomas F. and Kate Miller Jeffress Memorial Trust through grant J-545.

VII. REFERENCES

- [1] M. van der Voort, C. W. Rella, L. F. G. van der Meer, A. V. Akimov, and J. I. Dijkhuis, *Phys. Rev. Lett.* **84**, 1236 (2000).
- [2] M. Budde, G. Luepke, C. Parks Cheney, N. H. Tolk, and L. C. Feldman, *Phys. Rev. Lett.* **85**, 1452 (2000).
- [3] Oxygen in Silicon: Semiconductors and Semimetals, edited by F. Shimura, *Semiconductors and Semimetals Vol. 42* (Academic Press, New York, 1994), and references therein.
- [4] W. Kaiser, P. H. Keck, and C. F. Lange, *Phys. Rev.* **101**, 1264(1956).
- [5] M. D. McCluskey, *J. Appl. Phys.* **87**, 3593 (2000)
- [6] H. J. Hrostowski and R. H. Kaiser, *Phys. Rev.* **107**, 966(1957).
- [7] D. R. Bosomworth, W. Hayes, A. R. L. Spray, and G. D. Watkins, *Proc. R. Soc. London, Ser. A* **317**, 133 (1970).
- [8] H. Yamada-Kaneta, C. Kaneta, and I. Ogawa, *Phys. Rev. B* **42**, 9650 (1990).
- [9] M. Budde, G. Luepke, E. Chen, X. Zhang, N. H. Tolk, L. C. Feldman, E. Tarhan, A. K. Ramdas, and M. Stavola, *Phys. Rev. Lett.* **87**, 145501 (2001).
- [10] G. Luepke, X. Zhang, B. Sun, A. Fraser, N. H. Tolk, and L. C. Feldman, *Phys. Rev. Lett.* **88**, 135501 (2002).
- [11] A. Nitzan and J. Jortner, *Mol. Phys.* **25**, 713 (1973); A. Nitzan, S. Mukamel, and J. Jortner, *J. Chem. Phys.* **60**, 3929 (1974).
- [12] C. Kittel, *Solid State Physics*, (1976)
- [13] W. J. Silfvast, *Laser Fundamentals*, (1996)
- [14] D. J. Griffiths, *Introduction to Quantum Mechanics*, (1995)
- [15] M. Budde, unpublished, University of Aarhus (1998)
- [16] S.A. Egorov and J.L. Skinner, *J. Chem. Phys.* **103**,1533 (1995)
- [17] M. A. Roberson, S. K. Estreicher and C. H. Chu, *J. Phys.: Condens. Matter* **5**, 8943 (1993).
- [18] C. Flensburg and R. F. Stewart, *Phys. Rev. B* **60**, 284 (1999).

- [19] D. D. Dlott in *Laser Spectroscopy of Solids II*, edited by W. M. Yen (Springer-Verlag, Berlin, 1989), Chap. 5.
- [20] A. J. Mayur, M. D. Sciacca, M. K. Udo, A. K. Ramdas, K. Itoh, J. Wolk, and E. E. Haller, *Phys. Rev. B* **49**, 16293(1994).
- [21] C. Parks Cheney, M. Budde, G. Luepke, L. C. Feldman, and N. H. Tolk, *Phys. Rev. B* **65**, 35214 (2002).
- [22] R. Jones and A. Umerski, *Phys. Rev. B* **45**, 11321(1992).
- [23] E. Artacho, F. Yndurain, B. Pajot, R. Ramirez, C. P. Herrero, L. I. Khirunenko, K. M. Itoh, and E. E. Haller, *Phys. Rev. B* **56**, 3820 (1997).
- [24] M. D. McCluskey and E. E. Haller, *Phys. Rev. B* **56**, 9502 (1997).